Land cover classification using LiDAR height texture and ANNs

QIAO Jigang[1,2], LIU Xiaoping[1], ZHANG Yihan[1]

1. *School of Geography and Planning*, *Sun Yat-sen University*, *Guangdong Guangzhou* 510275, *China*;
2. *Resource and Environment School*, *Guangdong University of Business Studies*, *Guangdong Guangzhou* 501320, *China*

Abstract: The method of strict slope threshold algorithm is not sufficient to achieve complex object identification or ground features classification from LiDAR data. In this research, artificial intelligence is used to classify the ground features based on the LiDAR height texture. Average elevation image, average intensity image and ground roughness index image are derived from LiDAR points. Then, 4 GLCM texture features including entropy, various, second moment and homogeneity texture are measured. Finally, BP-ANNs are used to classify the texture measure into five ground feature types. A coastal area of Zhujiang Delta, South of China, is taken as the study area. The method employed in this research can efficiently work with single LiDAR data source and the accuracy of classification result is > 90%, and the classification accuracy of Maximal Likelihood method (ML) is 86.8% for comparison. When the result of ANNs classification is compared with the result of optical image classification, it can be found that 76.5% sample points are in accord.

Key words: LiDAR, height texture, Artificial Neural Network (ANNs), ground roughness index, classification

CLC number: TP751.1 **Document code**: A

Citation format: Qiao J G, Liu X P and Zhang Y H. 2011. Land cover classification using LiDAR height texture and ANNs. *Journal of Remote Sensing*, **15**(3): 539–553

1 INTRODUCTION

LiDAR (Light Detection And Ranging) is an active remote sensing system that uses the near-infrared laser to measure the distance between the sensor and target on the Earth surface. LiDAR data is composed of a mass of discrete points with high density and irregular distribution. Besides the location information of ground objects, height difference and 3-dimension features of ground objects can be derived from LiDAR point clouds directly. The initial tasks of applying LiDAR data is for fast ground survey as well as to separate ground and objects from point clouds and generate the Digital Elevation Model (DEM) and 3D building models.

In the past decade, researchers have presented many algorithms to extract the ground objects from LiDAR data. Kraus and Pfeifer (1998) have used an iterative linear prediction scheme for removing vegetation points in forested areas. Axelsson (1999) has presented a self-adaption triangulation network algorithm for filtering and classification of data points. In these algorithms, the triangulation network or line are constructed inside the points set based on the adjacent points slope threshold value, and used as a point clouds segmentation boundary. All the algorithms based on slope threshold value are exact segmentation measurements at any point clouds part, and usually employ to generate DEM or Digital Terrain Model (DTM). However, the exact segmentation measurement cannot adapt the complex objects identification because these objects may be composed by different classes points, and there are always points which cannot be classified solely relying on the LiDAR data itself. Therefore, when LiDAR points are used as source data of land cover classification or complex objects identification, the algorithms based on fuzzy measurement and intelligent identification tools are needed to cluster and classify the LiDAR points.

In recent years, researchers have brought out a series of LiDAR height texture measurements. Instead of the model classifying the points by slope threshold value, height texture measures are elevation statistics feature of LiDAR points in a floating detecting scene. Height texture of LiDAR is a fuzzy description of the spatial structure of elevation and slopes. Maas (1999) has used height texture for segmentation of LiDAR data. Filin (2002) has proposed a surface clustering technique for identifying regions in LiDAR data that exhibit homogeneity in a feature space consisting of tangent plane and relative height difference attributes. Most of the previous work on height textures classification of LiDAR data has concentrated on unsupervised clustering which are not effective in complex objects identification, but it shows that the height textures have potential capability in fuzzy measurement.

Defining height textures of LiDAR data and choosing textures identification model are key technologies in LiDAR classification. And considerable studies have been carried out in recent years.

Received: 2009-12-01; **Accepted:** 2010-08-17

Foundation: The National Natural Science Foundation of China UnderGrant (No. 40901187); The Guangdong Provincial Natural Science Foundation of China (No. 9451027501002471)

First author biography: QIAO Jigang (1973—), male, Ph.D., his research interests are LiDAR data processing and application, Geo-simulation system, CA simulation and application. E-mail: qjg821@263.net

Corresponding author: LIU Xiaoping, E-mail: yiernanh@163.com

Dimitrios and Keith (2007) has presented a multi-scale textured-based algorithm for object identification and DEM generation from LIDAR data. Poonam and Tiwari (2008) has applied a knowledge-based expert system to analysis the LiDAR texture information and implemented urban buildings identification. Jungho, *et al*. (2008) has explored the applicability of high-posting-density LiDAR texture based on height information and of land cover classification using machine-learning decision trees. Most pervious researches focus on one or two typical ground objects identification, or LiDAR data usually was used as ancillary data to improve land cover classification accuracy. When LiDAR data used as the sole information source or applied to land cover classification in complex ground conditions, classification precision resulting from traditional unsupervised classification method still need to be improved. The rapid development of artificial intelligence science improve the pattern recognition technology obviously which have been applied for remote sensing classification in the past decade (Liu, *et al*., 2008). However, the potential and validity of artificial intelligence model for LiDAR height textures recognition have been investigated rarely. In short, the researches of LiDAR height textures model definition and of employing stable and generalizable classifiers for height textures identification are in initial phase.

In this research, we focus on the validity of artificial intelligence method for LiDAR texture-based land cover classification. This paper presents Ground Roughness Index (GRI) as a new measurement for LiDAR height textures. Combining the GLCM textures, laser return intensity data with GRI in a feature space, the height textures are used for land cover multi-class judgment. Back Propagating Artificial Neural Network (BP-ANN) is employed as a classifier because it is capable to approximate any non-linear relationship by continuous or intermittent signal propagation among the neurons. BP-ANN can be used to signal processing, model identification as well as the remote sensing date classification. In this research, pixels from 5 land cover classes are sampled from height texture images: water body, buildings, high trees, bare land and grass ground, and they are used in BP-ANN training. The precision of LiDAR data classified by BP-ANN is higher than the result from Maximal Likelihood classifier (ML). At last, the result of ANN classification is compared with the result of spectral image classification.

2 METHODOLOGY

2.1 Transfer LiDAR discrete points to height image

It is hard to obtain the textural information directly from LiDAR irregular discrete points. These discrete points need to be transferred to surface model for texture measurement. Original LiDAR data include all the ground objects points, from which the Digital Surface Model (DSM) could be built. Unlike DEM, DSM is a superposition model of the hypsography and the height of the ground attachments. In other words, it is a surface model composed of all the observed subjects. During the transformation process from LiDAR discrete points to DSM, sample step L is obtained from the average density of the laser foot points, *i.e*. $L^2=S/n$. S stands for area of the whole survey area, and n stands for the number of the foot points. Since the distribution of the foot points are often irregular, the number of the foot points in a specific sampling grid may exceed 1, or equal to 1, or with no foot point at all. In addition, two types of data are found in LiDAR foot points: elevation and return intensity data. When the number of the foot point exceeds 1, the cell values of elevation and the return intensity are the mean values of elevation and the return intensity. When there is no foot point in the grid, the cell values of the elevation and the return intensity are different: the elevation value is the minimum of the neighborhood, and the intensity value is zero. Therefore DSM can be obtained when the grid takes the value of the elevation and then the height image (depth image) could be derived from DSM. Likewise, the intensity image is obtained when the return intensity value is assigned to cells.

2.2 Texture measurement

Height texture is texture measurement of LiDAR height image. Height texture is also the major information of LiDAR land cover identification. Alongside the height textures, the value of mean return intensity and mean height are also seen as the features used in land cover classification.

2.2.1 Height textures based on the GLCM

Grey-Level Co-occurrence Matrices (GLCM) also is used in this study, which is based on brightness value spatial-dependency (Haralick, *et al*., 1986). GLCM is a probability matrices of pixel grey levels occur in a detecting scene. The GLCM textures have been widely used in remote sense image segmentation and object identification (Franklin, *et al*., 2001). Companying with last return information, 5 from all 14 GLCM textures were used to ground object identification from LiDAR height image by Jungho, *et al*. (2008). In this study, 4 GLCM textures, including Homogeneity (*H*), Various (*V*), Entropy (*En*), and Second Moment (*ASM*), are employed as ground features for classification. As well as, Means gray value (*M*) is calculated as a texture measurement. Table 1 demonstrates the methodologies of GLCM textures measurements employed in this paper.

Table 1 Texture measure methodologies

Metric	Equation	Description
Various	$V=\frac{\sum(p(n)-M)^2}{n-1}$	M=mean DN value of floating detecting scene
Second moment	$ASM=\sum_i\sum_j\left[p(n)\right]^2$	ASM is the depiction of the height texture distribution
Entropy	$En=-\sum_i\sum_j p(n)\lg p(n)$	En indicates variation of height in a detecting scene
Homogeneity	$H=\sum_i\sum_j\left(\left(\frac{1}{1+(i-j)^2}\right)\frac{p(n)}{\sum_i\sum_j p(n)}\right)$	H weights the values decreasing exponentially according to their distance to the diagonal

Note: $p(n)$ = the DN value of pixel, and i, j = the number of rows and columns.

2.2.2 Ground roughness index

LiDAR data used in this research only has single return record. For the purpose of measuring the globe height statistic feature, we propose Ground Roughness Index (GRI, C_p) which defined by the area ratio of the DSM and DEM in a detecting scene:

$$C_p = \frac{\sum_{i=1}^{n} S_{i\mathrm{DSM}}}{\sum_{i=1}^{n} S_{i\mathrm{DEM}}} \quad (1)$$

where n is the total grid number in a detecting scene, $S_{i\mathrm{DSM}}$, $S_{i\mathrm{DEM}}$ are area of DSM and DEM in grid i.

In our experiment, the detecting scene use 7×7 volume, and n=49. DEM is derived from ground points which segmented from LiDAR point clouds by self-adaption triangulation network algorithms (Axelsson, 1999). When C_p is used as a height texture measurement for ground identification, its operational reliability depend on the precision of DEM. Based on our experiment, the precision of DEM is enough when the ground points come up to 10% in whole LiDAR points in flat area. Fig. 1 is a sketch map shown the relationship between DSM and DEM section. The value of GRI could be approximately interpreted as the length ratio of DSM and DEM line segment in sketch map.

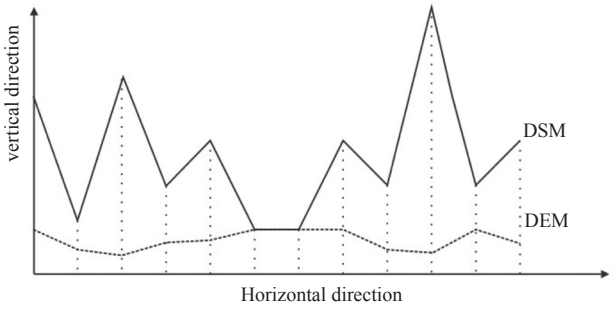

Fig. 1 DSM and DEM section

C_p is insensitive to ground repetitive structure and detecting direction, but the hypsography and the height changes of ground attachments have an effect on the value of C_p obviously. It can be seen from formula 1 that the height change of land cover, such as buildings, trees, is the main factor of GRI because DSM overlaps above the DEM. In fact, bigger the hypsography changes and height changes are, greater the area of DSM is, and greater the value of C_p is. So, the type of land cover or ground objects can be identified according to the C_p value. For example, while the trees and buildings have similar height changes, the C_p value of woodland is greater than the C_p value of buildings because only few LiDAR points falling on the ground gap between trees will increase the area of DSM obviously. So, we can distinguish the buildings from woodland by C_p value. While woodland and grassland have similar undulate distribution on the ground, the C_p value of woodland will greater than the grassland because trees have greater height change. Therefore, C_p can be interpreted as a ground feature of total height changes measurement, and can be used to land cover classification.

2.3 Land cover classes

The classes of land cover are persetted according to the separability of height textures. LiDAR data is a kind of elevation records about ground or ground attachment. Elevation value or height differences are the main information applied to land cover classification. Though there have return intensity records in LiDAR data, the intensity data cannot be used as sole information source for land cover classification because of its low radiation and spectrum resolution. Therefore, land cover classes should be discernible on height features firstly, and return intensity records are used only as secondary basis. So, 5 classes of land cover in study area are chosen mainly based on the height features: water body, buildings, woodlands (high trees), bare lands, farmlands (or grasslands). In these classes, buildings usually have relatively great height and low GRI value, high trees or woodlands have similar height with buildings but great GRI value. Both of the height value and GRI value are low in bare land and middling in farmlands. Water body is always on lowland with low return intensity. All these features can be discerned from height textures and used for land cover classification.

2.4 BP-ANN work models and process

Artificial Neural Networks (ANNs) are a functional abstraction of the biologic neural structures of the central nervous system. ANNs are trainable architecture and are operated as black-box, model-free, and self-adaption tools for learning knowledge form the sample-training. They are powerful pattern recognizers and classifiers. Using neural network, the detection rule of object can be derived from high-dimensional feature space. During the past decade, ANNs have been wildly used in remote sensing applications, especially in the field of image classification (Minh, *et al*., 2005). Back Propagation algorithm is a machine learning technology widely applied in multilayer feed forward network. Steepest error descent method is used to modify the weight coefficient and to improve the accuracy of solution in BP algorithm. This algorithm is stable, fault tolerant and robust, and it is capable for LiDAR height texture identification.

BP network is composed of input layer, hidden layer and output layer. While in one loop of training process, the sample data, coming from input layer and then going through hidden layer, arrive to output layer at end. Nerve cells in input layer and hidden layer only have influence on the next layer. The errors which are the deviation between truth value and working value are calculated in output layer. Then, errors signals are propagated backward alone the cell connection, and steepest descent method is used to modify weight coefficient between the nerve cell one by one. Repeat this loop, and stop iteration till the errors descent to a predetermined threshold value. Classifying rules has been built after training. The function of nerve cell in hidden layer and output layer could be expressed as follow (Qing and Lu, 2000):

Given x_i is the input value on i input cell, the output value of the cell j in the hidden layer y_j could be expressed as follows.

$$y_j = f\left(\sum_i W_{ij} x_i + \theta_j\right) \quad (2)$$

where W_{ij} is the connect weight coefficient between cell i in input layer and cell j in the hidden layer, θ_j is the threshold value of the hidden cell j. Transfer function used in nerve network is Sigmoid function and is expressed as follows.

$$f(x) = 1 \Big/ \left(1 + \exp\left(-\frac{x}{\theta_0}\right)\right) \quad (3)$$

where θ_0 is used to adjust the sigmoid function. And the output of cell k in hidden layer (O_k) can be expressed as follows.

$$O_k = f\left(\sum_j V_{kj} y_i + \sigma_k\right) \tag{4}$$

where V_{kj} is weight coefficient between the cell j in hidden layer and cell k in output layer, σ_k is output value of cell k in output layer. Steepest errors descent method is used to estimate and modify weight coefficient matrix. Learn ratio of ANN is given by user. Errors function ε can be expressed as follows.

$$\varepsilon = \frac{1}{2}\sum_{i=1}^{N}\sum_{k=1}^{P}(O_{ik} - T_{ik})^2 \tag{5}$$

where O_{ik} is the actual output. T_{ik} is the desired output. P represents the number of output cells. N represents the number of samples.

Fig. 2 show the flow diagram of the methodology used in the study.

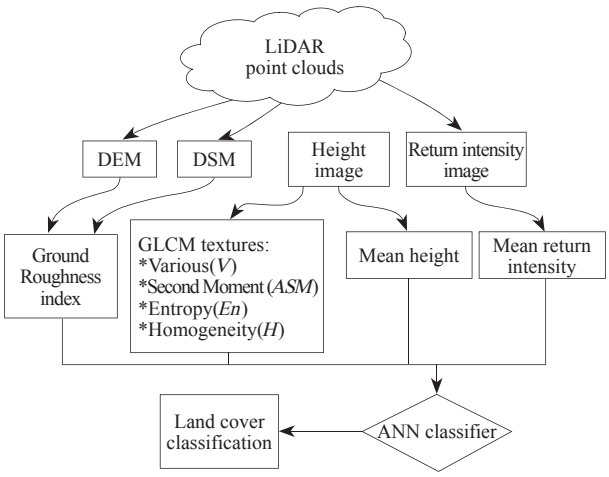

Fig. 2 Workflow used in study

3 EXPERIMENTS

3.1 Study area

In this study, we are focusing on a 3.5 km^2 coastal zone in Zhujiang Delta, South of China. Study area is local in a fame belt with in general less 2 degree terrain variance. A small village is in northwest corner of study area. Common height of buildings is less than 10 m; the height of high trees is similar with buildings and overlay with buildings somewhere. Water body includes several ponds and a creek with obvious stream ditch. Bare land, grass land, cropland and dwarf shrubbery can be found in this area also.

3.2 Data process

LiDAR data were collected on November 14, 2006 using Leica Airborne Laser Scanner 50 sensor. The LiDAR operated at near-infrared spectrum with first return record, the average sampling distance among footprints is approximately 0.78 m. Max altitude difference is 13.16 m among whole points, and the elevation of 94% points is less than 6 m. Coordinate has been provided in UTM projection with an absolute accuracy of < 0.8 m in the x and y directions, and < 0.15 m in the z direction. Reflect intensity of returns is recorded as 10 grades also. Using TerraSolid software, LiDAR points are segmented into two parts: ground points and non-ground points by slope threshold at 2 degree iteration angle. DEM and DSM are generated respectively from ground points and whole the points with 0.8 m grid. TerraScan software is used to transfer grid to grey images respectively according to the elevation value and reflection intensity value. Then, these gray images are stretched to 256 gray scales and shown as Fig. 3.

(a) (b)

Fig. 3 Grey images derived from LiDAR data
(a) Height image; (b) Return intensity image

After a number of experiments, 7×7 detecting scene is chosen with the best performance in following classification. The area of one scene is 5.6 m×5.6 m in actual ground, similar with or little smaller than the area of buildings. 4 GLML height texture measures are calculated following the Table 1. Ground roughness can be obtained from formula 1. Images of the 4 GLML textures and GRI are shown in Fig. 4.

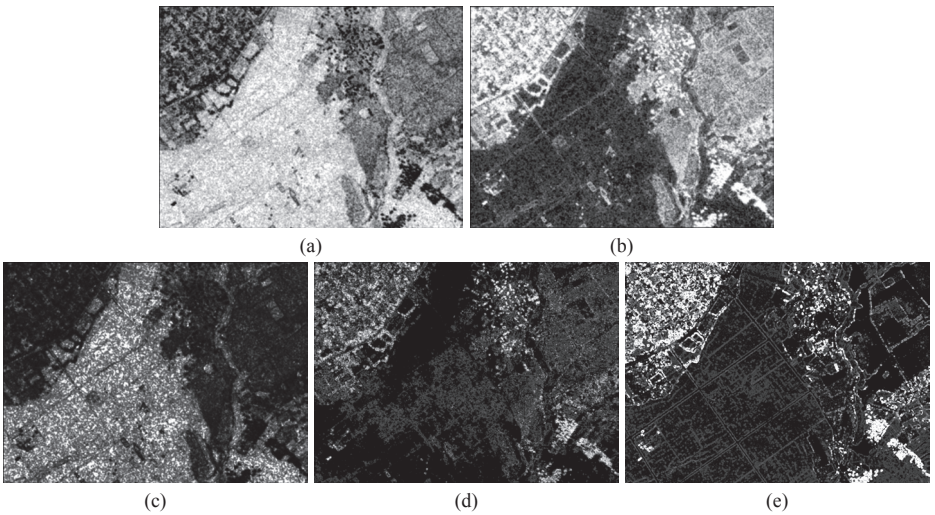

(a) (b)

(c) (d) (e)

Fig. 4 Height texture measures
(a) Entropy (En); (b) Homogeneity (H); (c) Second Moment; (d) Various (V); (e) GRI (C_p)

3.3 ANNs training

A 3-layer BP-ANN are established. The software is developed by C#. 4 GLCM height textures, mean intensity, mean elevation and GRI are obtained. These 7 textures are inputted into the corresponding 7 neural cells in input layer. There are 4 cells in the hidden layer and 5 cells in output layer. The cell numbers of hidden layer are determined by experience. The cells number of output layer is corresponding to 5 target classes. Balance samples are applied for the training, which requires similar number of samples in each class. The average deviation is 1.96, showing good separability of samples. In the BP-ANN, Sigmoid function is used, with a training ration of 0.1. Train the network with training data set. And then the working data sets are inputted into network for classification after training.

4 RESULTS AND ANALYSIS

4.1 Results

The classification is shown in Fig. 5(a). The confusion matrix for classification error is shown in Table 2. The total accuracy of the classification is 90.22%. The most classification errors are found with the building class with an accuracy of 79.6%. 100% classification precision is achieved in bare lands and water body classes, due to the low altitude of water and the least terrain variations of the bare land. Furthermore, eyes judgment can tell that the classification errors are shown mainly in the top-left of map, where buildings and woodlands are mixed. The buildings in the region are mostly low, detached houses with similar height of the woodlands. Therefore the texture measurements are similar, especially on edges of object, and easily confused by BP-ANN classifier. The sparsely distributed grasses along the creek are identified as bare lands. Streamlet where is shallow and slight shape cannot be detected in a complete detecting scene. Therefore, these kinds of patches cannot be identified correctly. Other large water body can be effectively detected by height textures and return intensity data.

Maximum Likelihood (ML) classifier is also employed to classify the same region (Fig. 5(b)). Confusion matrix for classification errors are also worked out (Table 3). It can be seen that both methods can provide satisfactory classification results. The classification precision of BP-ANN for total validation samples is 90.25%, 3.5% higher than that of ML (86.75%). The Kappa of BP-ANN classifier is 0.877, also higher than that of ML method which is 0.832. Besides, the land cover patches obtained from ML classifier, especially where the buildings-woodlands and the grasslands-bare lands interleaving are more fragmented than the patches obtained from BP-ANN. it shows that BP-ANN has better performance in multi-attributes analysis and has stronger generalization ability. According to Fig. 2 and Fig. 3, the numbers of misclassified samples among classes are significant different in different classifier. Both classifiers show the least classification precision in buildings due to the overlaps of buildings and woods, and their similar heights. The accuracy of BP-ANN in buildings class achieves 79.6% while ML is only 22.22% which can hardly been regarded as valid identification. BP-ANN, with almost all the misclassified simples on buildings classes, has achieves the accuracy of 72.3 % and 97.4% in woodlands and grass lands respectively, slightly lower than that of ML classifier. In general, compared to ML classifier, BP-ANN model is capable in stability and fault tolerance, and thus fits in better with the LiDAR height textures classification.

Table 2 BP-ANN classification confusion matrix

	Buildings	Water body	Woodlands	Grasslands	Bare land
Buildings	43	0	18	2	0
Water body	0	46	0	0	0
Woodlands	8	0	47	0	0
Grasslands	3	0	0	76	0
Bare land	0	0	0	0	74
Total	54	46	65	78	74

Note: Total accuracy: 90.22%, Kappa=0.877

Table 3 ML classification confusion matrix

	Buildings	Water body	Woodlands	Grasslands	Bare land
Buildings	12	0	0	0	0
Water body	0	46	0	0	0
Woodlands	35	0	65	0	0
Grasslands	7	0	0	78	0
Bare land	0	0	0	0	74
Total	54	46	65	78	74

Note: Total accuracy: 86.75%, Kappa=0.832

4.2 A comparison between LiDAR height image classification and ALOS image classification

LiDAR land classification mainly bases on the height variance of land objects. But both the radiation resolution and spectral resolution are low in LiDAR data. Most of the laser receiver including ALS50 sensors can only have several radiation flux grades and sole spectral band (In this research, there are only 10 radiation flux grades). The original reflection data cannot be used to segment the point clouds directly. At present, traditional multi-spectral image is the major means in remote sensing survey. In real work, LiDAR is often used as a complement or reference to multi-spectral remote sensing data. Thus, we also use multi-spectral image to classify the land covers of the same region, and a comparison is made between the two results.

ALOS image of the region is chosen. The data is collected two months later than the LiDAR data. ALOS images are obtained using ALOS AVNIR2 and PRISM sensor. 4 band multispectral images and panchromatic image are used with resolution of 10 m and 3 m respectively. Borvey fusion method is used in data fusion with the best visual results and identifying accuracy (Liu, *et al*., 2008). After resampling the image with 0.8 m, ALOS image is classified by ML classifier. And the result is shown as Fig. 6.

Total 500 pixels (every 100 pixels in each class) are chosen from LiDAR classification result randomly and checked their classes in ALSO classification image. We contrast classification results from ALOS and LiDAR data, shown as error confusion matrices in Table 4. It can be seen from Table 4 that classification errors occur in each two classes. A total of 264 pixels with accuracy of 52.8%

Table 4 Classification conformity of ALOS image and LiDAR height image

		LiDAR height image classification						Conformity / %
		Buildings	Wood lands	Grass lands	Bare land	Water body	vegetation*	
ALOS image classification	Buildings	23	4	11	18	4	15	23
	Woodlands	40	67	17	11	5	153**	67
	Grasslands	24	15	54	6	9		54
	Bare land	8	11	16	61	23	27	61
	Water body	5	3	2	4	59	5	59

* composed by grasslands and woodlands class ** the number of vegetation samples is 200,with 76.5% conformity

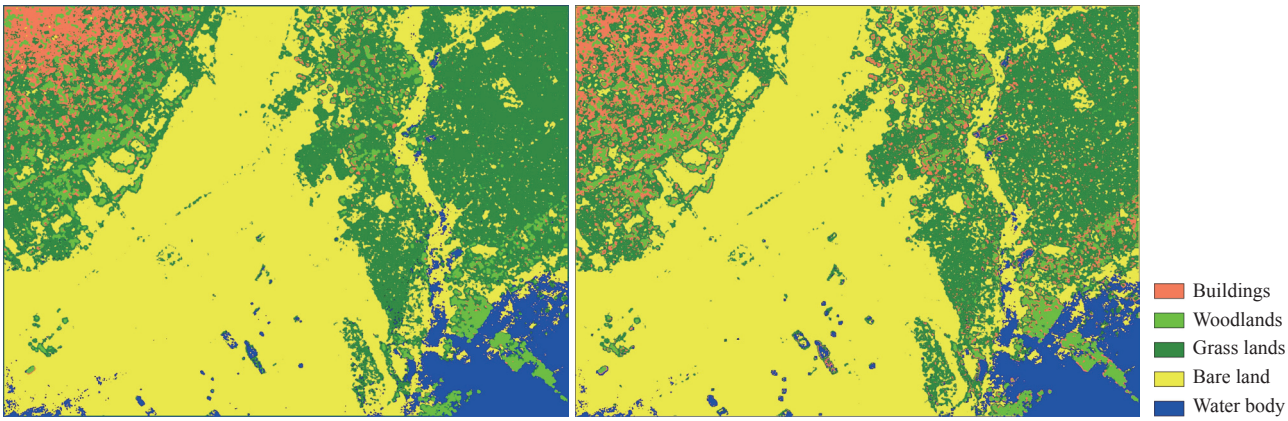

(a) (b)

Fig. 5 Results of classification
(a) BP-ANN classification; (b) ML classification

are the same classes in both image. Except buildings, about 60% conformity obtained in all other classes. Comparing Fig. 5(a) with Fig. 6 by eyes judgment, classifying confusion almost distributes between the classes of buildings and woodlands on the up-left corner of the map. According to our field survey, the buildings and trees there have similar height and overlap each other, there are large numbers of mixed pixels in the conditions of ALOS image's lower resolution than LiDAR height image's, which could cause classifying confusion obviously.

It is notable that the classifying conformance of the two data source has connection with the presetted classes. For example, it is hard to take the dwarf shrub, woodland and grassland apart from spectral image because all they are vegetation with similar reflection spectrum. However, when combining them into the class of vegetation, 76.5% pixels of vegetation identified from LiDAR data and ALOS image are in accord. Besides, the hard bare ground or road, which cannot be segmented in LiDAR data, can be identified in spectral image.

Furthermore, LiDAR data resolution and physical mechanisms of LiDAR scanner is different from spectral data. The classes chosen in advance and classifying strategy have significant influence on results of classifying conformance. A suitable ground conditions and classification schema is needed in this experiment. It is possible that the results of classifying are not comparable entirely in different conditions. This experiment is designed to test validity of LiDAR classification. However, the rational aims using LiDAR data and spectral data together usually are to enhance the image understanding and to improve classifying precision, but not only to obtain results with high conformity.

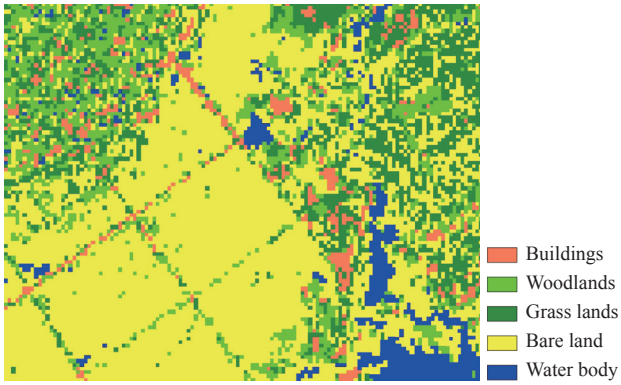

Fig. 6 Classification result of ALOS image

5 CONCLUSIONS AND DISCUSSION

(1) LiDAR point clouds provide information in elevation, height difference and reflection intensity. In this research, discrete points are transformed into height images and intensity images. Classification rules are drawn from the height textures by using the image segmenting techniques. The main information used in height textures classification is the same with the information used in vector point clouds segmentation. Both employ the height difference data of the foot points. Yet, the height textures are more fault tolerant and fuzzier in feature measurement, it is better for complex land cover identification. In the research, ground roughness index (GRI) and the return intensity offer assistant informa-

tion for classification. Experiments show that by using height textures, return intensity and ground roughness index, effective identification and classification of land cover can also be achieved without other data source.

(2) LiDAR height texture is more effective in land cover identification than height variance taken directly from discrete points. Besides, the features of the land cover shown in height textures are more distinct and comprehensible than that shown in discrete point clouds. ANNs is an effective tool in land cover classification form LiDAR data by seeking the rules in high dimension feature space. And in our experiment, ANNs has higher classification precision than Ml classifier. Artificial intelligence model can achieve better performance than traditional model in height texture identification.

(3) When comparing the results of height texture classification and the spectral data classification, it can be found that the conformity of classification is between 23% and 67%, with the total conformity of 52.8%. Therefore, it cannot be used as direct reference to each other. However, when woodland and grassland are combined into one class, vegetation, a higher conformity (76.5%) is found (Table 4). Taking the difference of image resolution into consideration, higher conformity is possible. And, the two classification results are comparable when designed classes and classifying strategy are suitable at same time for both LiDAR and spectral data in land cover identification.

(4) Since height variance of the ground is the main information of LiDAR, the classes presetted must be classifiable in elevation or height difference. Ground prior knowledge is also implicit in LiDAR texture based classifying strategy. The study area of this research is small, and the ground structure is simple. It is easy to choose classes in advance only depending on experience. But in conditions of complex terrain or complex ground attachments, or the researchers lacking of ground knowledge, significant errors are to be expected. Object-based technology and other intelligence models have the potential to reduce these errors in LiDAR height texture identification, which can be the field for further research.

Acknowledgements: We thank Prof. Li Xia for helpful suggestion in our study; also thank M. Wu Qiusheng, Dr.Ai Bin and Dr. He Jingqiang for providing documents and data support.

REFERENCES

Axelsson P. 1999. Processing of laser scanner data-algorithms and applications. *ISPRS Journal of Photogrammetry and Remote Sensing*, **54**: 138–147

Dimitrios C and Keith A. 2007. A texture-based technique for DEM generation from LIDAR data. Proceedings of SPIE, 6550, 65500O. DOI:10.1117/12.719935

Filin S. 2002. Surface clustering from airborne laser scanning data. *International Archives of the Photogrammetry, Remote Sensing and Spatial Information Sciences*, **34** (Pt. 3A): 119–124

Franklin S E, Maudie A J and Lavigne M B. 2001.Using spatial co-occurrence texture to increase forest structure and species composition classification accuracy. *Photogrammetric Engineering & Remote Sensing*, **67**(7): 849–855

Haralick R M.1986. Statistical Image Texture Analysis. Handbook of Pattern Recognition and Image Processing. New York: Academic Press

Jungho I, John R and Michael E. 2008. Object-based land cover classification using high-posting-density LiDAR data. *GIScience & Remote Sensing*, **45**(2): 209–228

Kraus K and Pfeifer N. 1998, Extraction of buildings and trees in urban environments. *ISPRS Journal of Photogrammetry and Remote Sensing*, **53**: 193–203

Liu W Y, He G J, Zhang Z M and Liu H C. 2008. Comparison of fusion algorithms for ALOS panchromatic and multispectral images. *Science Technology and Engineering*, **8**(11): 2864–2869

Liu X P, Li X, Liu L and He J Q. 2008. An innovative method to classify remote-sensing images using ant colony optimization. *IEEE Transactions On Geoscience and Remote Sensing,* **46**(22): 4198–4208

Maas H G. 1999. The potential of height texture measures for the segmentation of airborne lasers canner data. Fourth International Airborne Remote Sensing Conference and Exhibition. Ottawa: 21st Canadian Symposium on Remote Sensing: 154–161

Minh Q, Nguyen P, Atkinson M and Hugh G L. 2005. Super-resolution mapping using a hopfield neural network with LIDAR data. *IEEE Geoscience and Remote Sensing Letters,* **2**(3): 366–370

Poonam S and Tiwari H P. 2008. Use of laser range and height texture cues for building identification. *Journal of the Indian Society of Remote Sensing*, **36**: 227–234

Qin Q M and Lu R J. 2008. Satellite image classification based on fractal dimension and neural network. *Acta Scientiarum Naturalium Universitatis Pekinensi*, **36**(6): 858–864

Raber G, Jensen J R, Hodgson M E, Tullis J A, Davis B A and Berglund J. 2007. Impact of LiDAR nominal posting density on DEM accuracy and flood zone delineation. *Photogrammetric Engineering & Remote Sensing*, **73**(7): 793–804

基于LiDAR高度纹理和神经网络的地物分类

乔纪纲[1,2]，刘小平[1]，张亦汉[1]

1. 中山大学 地理科学与规划学院 遥感与地理信息工程系，广东 广州 510275；
2. 广东商学院 资源与环境学院，广东 广州 501320

摘 要：使用LiDAR单一数据进行点云分割工作时，基于斜率的严格分割LiDAR点云的方法不能很好的适应复杂地物的分类工作。本文将LiDAR粗分割后的点云转换为高度图像和反射强度图像，并求取高度图像GLCM高度纹理。将4种GLCM高度纹理、地面粗糙系数、平均高度和平均反射强度共7种纹理作为识别地面覆盖物的特征,并利用后向传播神经网络(BP-ANN)方法对LiDAR数据进行地物识别。实验表明，这种方法能够从LiDAR独立数据源中有效的实现地物分类，实验获得的精度大于90%。与传统的最大似然法进行对比,BP-ANN的分类精度高于最大似然法。当预设地面类型能同时满足被光学影像和LiDAR数据识别的条件时，LiDAR高度纹理分类与光学影像分类结果的一致性达到76.5%。

关键词：LiDAR，高度纹理，人工神经网络，地面粗糙度，分类

中图分类号：TP751.1 **文献标志码**：A

引用格式：乔纪纲，刘小平，张亦汉. 2011. 基于LiDAR高度纹理和神经网络的地物分类. 遥感学报，**15**(3): 539–553
Qiao J G, Liu X P and Zhang Y H. 2011. Land cover classification using LiDAR height texture and ANNs. *Journal of Remote Sensing*, **15**(3): 539—553

1 引 言

LiDAR (Light Detection And Ranging)是一种主动光学遥感系统，它采用近红外波段激光测量目标和传感器之间的距离。LiDAR数据是一种不规则的高密度离散点结构，地表特征信息特别是那些受高度控制的要素可以利用LiDAR点云(point cloud)的空间分布计算得到。LiDAR数据最初是用于快速地形测量、DEM生产以及3维城市建模等领域Raber等，2007；针对这些应用领域，已经发展出许多分割地面—非地面点的算法，包括相邻点间迭代角线性预测方法(Kraus和Pfeifer，1998)、自适应不规则三角网分割等(Axelsson，1999)。这些算法是直接针对离散点工作，用三角网或直线构建相邻点关系并计算用于分割的斜率，由此获取高精度的DEM和DSM模型。基于斜率变化的点云分割算法对每个测点局部上都能取得严格的划分，但通常仅用于数据预处理和DEM建模。当面对由不同类型点构成的复杂地面对象时，该方法不能有效地进行地物识别。因此，对大范围、多类别或复杂地物的识别问题，需要使用更为模糊的特征测度和更为智能的模式识别工具。

近年来，一系列适用于LiDAR高度图像纹理特征的方法被提出，用区域内高度变化的统计特征来分割点云，而不是仅仅依靠某个点的高度值。Mass(1999)最早将测点高度变化的统计特征定义为高度纹理(Height Texture)，是指检测窗口内由LiDAR点群(point set)高程所定义的灰度像元的数量和质量的组合模式。Filin(2002)提出了一种表面聚类算法，该算法采用LiDAR测点到一个切平面的相对高度来计算某个窗口内测点的同质性，并据此对LiDAR测点作出分割。该算法仍然是一种严格划分

收稿日期：2009-12-01；**修订日期**：2010-08-17

基金项目：国家自然科学基金 (编号：40901187)；广东省自然科学基金资助项目(编号：9451027501002471)

第一作者简介：乔纪纲 (1973—)，男，讲师，中山大学博士，主要研究方向为激光雷达数据处理与应用、遥感信息模型以及地理模拟系统。E-mail: qjg821@263.net。

通信作者：刘小平，E-mail: yiernanh@163.com。

方法，但引入了高度纹理的思想，采用窗口内点群高度的统计特性来分割点云。大多数早期工作主要采用了非监督分类方法，尽管对复杂对象的分类效果不太理想，但显示出高度纹理用于模糊特征表达的有效性和潜在应用价值。

定义高度纹理的测度以及对这些测度的有效识别，是利用高度纹理分割点云的两个关键技术。近年来，已有学者在这两方面进行了初步的探索。Dimitrios和Keith (2007)提出了一种多尺度的高度纹理特征，用于基于地貌形态特征的LiDAR高度图像分割。Poonam和Tiwari (2008)采用基于知识的专家系统对LiDAR高度纹理特征建立分类规则，并用于城市建筑的识别；Jungho等(2008) 则在研究中引入了决策树方法对高度纹理特征进行识别。已有的研究中，大多是针对特定目标(如建筑或微地貌特征)构建高度纹理特征并进行识别和分类，此时一般分类方法能够满足精度的要求。但是，当地面条件复杂或进行多类分类的时候，用常规的分类方法单独对高度纹理识别，精度还有待提高。目前，随着人工智能技术的发展，遥感分类也趋向与智能化技术相结合(Liu 等，2008)；但是将人工智能算法引入到LiDAR高度纹理识别的研究还很有限。如何利用LiDAR数据特点来构造适当的高度纹理，并根据这些高度纹理选择具有稳健性和推广能力的分类器来提高分类精度。目前，在这两方面还有大量的工作有待深入。

本文的工作是围绕着高度纹理特征提取和引入高度纹理的智能分类算法展开。研究中，在斜率阈值分割点云的基础上，构造了地面粗糙系数作为一种高度纹理；与GLCM纹理和反射强度共同构成特征空间用于多类地物分类。在智能算法方面，本文尝试引入后向传播神经网络(BP-ANN)进行LiDAR高度纹理特征识别。人工神经网络(Artificial Neural Network，ANNs)是由人工建立有向图拓扑结构的动态系统，能够以神经元为单位通过连续或断续的工作方式，充分逼近任意复杂的非线性关系；能较好地适应模式识别和信号处理等方面的问题，且在遥感图像分类中有广泛应用。实验中，通过BP算法训练ANNs并定义分类规则，将地物分为水体、人工建筑、林地、草地和裸地5种类型。实验结果的分类精度优于最大似然分类，且与光学遥感影像的分类结果具有可比性。

2 方 法

2.1 LiDAR离散点云转换为栅格图像

不规则离散点之间的空间关系难以直接获取纹理信息，需要转换为表面模型并以规则格网进行表达。原始LiDAR点云包含全部地面对象，直接建模得到的表面模型被称为数字表面模型(Digital Surface Model，DSM)。DSM与数字地面模型(DEM)不同，它是地形起伏变化和地物高度变化的叠加，即由全部被观测对象构成的表面模型。从LiDAR离散点云转换为DSM过程中，采样宽度L由区域内激光足点的平均密度求得，即：$L^2=S/n$，S为区域面积，n为激光测点数。但由于测点是不规则分布，某个格网内的测点数存在多于1个、等于1个和没有测点3种情况；此外，LiDAR测点也还有高程值和反射强度值两种数据。当网内的足点数多于1个时，高程和强度值取平均值；当格网内没有足点时，高程和反射强度取值方法不同：格网高程值取其邻域格网的最小值；反射强度值取0。当格网按高程取值时即可得到DSM，用栅格表达得到地面高度图像；按反射强度取值后用栅格表达则得到地面反射强度图像。

2.2 纹理特征提取

高度纹理是对高度图像求取的纹理特征，是在检测窗口内地面对象高程变化的统计。高度纹理也是LiDAR识别地面对象的主要信息来源。除高度纹理外，检测窗口内的平均反射强度和平均高度也作为地物的特征参与分类。

2.2.1 基于GLCM的高度纹理

灰度共生矩阵(GLCM)是一种纹理度量工具(Haralick，1986)。它是根据像元灰度分布计算出的统计概率矩阵，被广泛的用于图像分割对象识别等领域(Franklin 等，2001)。GLCM提供了14种纹理，Jungho等 (2008) 使用了5种GLCM高度纹理并结合LiDAR末次反射(Last Return)信息对地面进行了识别。我们经过多次实验，选取4种GLCM高度纹理就能够取得较好的分类效果，分别是：变异系数(V)、二阶矩(ASM)、信息熵(En)和图像同质性(H)。这些纹理值均按窗口的4个正方向取平均值求得；此外，平均灰度(M)也作为一个纹理特征被计算出来。图象纹理的计算方法如表1所示，表中$p(n)$为像元的DN值，i，j为规定检测方向上像元的行、列号。

表1 纹理计算方法

纹理特征	计算式	注
变异系数	$V=\frac{\sum(p(n)-M)^2}{n-1}$	M为移动窗口的平均DN值
二阶矩	$ASM=\sum_i\sum_j[p(n)]^2$	描述了图像灰度分布均匀程度和纹理粗细度
信息熵	$En=-\sum_i\sum_j p(n)\lg p(n)$	描述了图像具有的信息量的大小
同质性	$H=\sum_i\sum_j\left(\left(\frac{1}{1+(i-j)^2}\right)\frac{p(n)}{\sum_i\sum_j p(n)}\right)$	描述了像元及其邻域灰度连续变化的强度和振幅

注：$p(n)$为像元的DN值；i、j分别表示行数与列数

2.2.2 地面粗糙系数

实验数据仅有一次反射(First Return)信息，为了度量地面对象的相对高度及其统计特征，我们设计了地面粗糙度系数(C_p)，并作为一个高度纹理特征参加分类。地面粗糙系数被定义为检测窗口内DSM面积与DEM面积的比值，由式(1)表达：

$$C_p=\frac{\sum_{i=1}^{n}S_{i\mathrm{DSM}}}{\sum_{i=1}^{n}S_{i\mathrm{DEM}}} \tag{1}$$

式中，$S_{i\mathrm{DSM}}$、$S_{i\mathrm{DEM}}$分别为DSM和DEM表面在第i格网内的面积，n为单元格网i的摩尔邻域数，n的取值由随后求取纹理特征的邻域数确定，在本文实验中采用了7×7的卷积，即n=49。DEM是由LiDAR点云得到的，利用自适应不规则三角网分割方法将LiDAR离散点云中的地面点分离出来(Axelsson，1999)，并从地面点构建DEM。值得注意的是，C_p作为纹理来反映地面特征的可靠性与DEM的建模精度有关系。根据经验，在地势较为平缓的区域DEM建模时，地面点占全部激光足点数10%左右即可。

图1显示了DSM和DEM的剖面分布示意。可以近似的认为地面粗糙系数是图中DSM线段长度与DEM线段长度的比值。

地面粗糙系数(C_p)对地面的重复结构不敏感，也没有方向性；但是对检测窗口内地面覆盖物起伏的密度和幅度敏感；而且由于DSM是叠加在DEM上的，图1中可以发现C_p主要与地物的起伏变化有关，

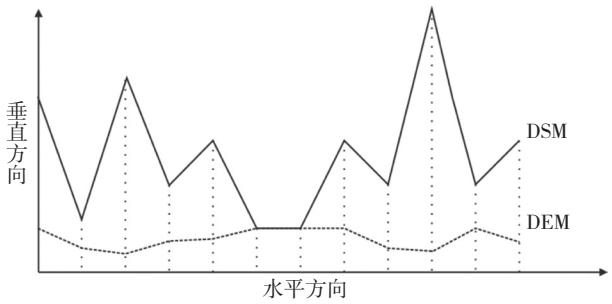

图1 DSM与DEM剖面分布

而DEM的起伏变化对C_p影响很小。地物的起伏越密集、高差越大则DSM面积越大，C_p也越大。可以据此来分离不同类型的地物。例如，高度相仿的树木和人工建筑，即使树木缝隙之间只有少量的激光测点落到地面上也能使得林地的C_p值远大于建筑；而起伏密度相当的林地和草地，由于林地测点间的平均高差较大，其C_p值也会大于草地的C_p值。因而，作为地物高差变化在一定区域内总体特征的度量，地面粗糙系数是地物识别的有效测度。

2.3 地面类型设定

地物类型是根据数据的可分性来设定。LiDAR数据记录的是地面高度信息，这也是用来识别地物类型的主要信息来源；尽管每个足点都有反射强度记录，但只有一个波段且反射强度的辐射分辨率较低，不适合单独使用。在设定地物类型的时候主要按其对高度变化敏感性来选择，地面反射强度作为辅助。根据这一原理我们针对实验区作出了5种地面覆盖物的划分：人工建筑(建筑)、林地(指高大树木)、草地(或农田)、裸地和水体。一般来说，建筑具有较大的相对高度和较小的粗糙度；林地有较大高度和粗糙度；裸地为较小的高度和粗糙度；农田取值均中等；水体有较小的反射强度和高度值等。利用这些特点可进行高度纹理识别和地物分类。

2.4 BP神经网络工作方法与数据流程

人工神经网络(ANNs)是生物神经系统的简约模型。ANNs具有可训练、模式自由、适应性强的特点，其过程为黑箱，用户无需了解神经网络内部过程；使用神经网络能够从高维特征空间中获取对象的分类规则，是一种有效的模式识别和分类工具。已有多种神经网络被用来进行遥感图像分类，也有许多成功的案例(Minh 等，2005)。后向传播(Back

Propagation，BP)算法是多层前馈网络使用最广泛的学习技术之一。该算法是按照误差最大下降梯度逐层修正权系数的方法来搜索最优解；具有较强的稳定性、容错性和鲁棒性，能很好的适应高度纹理识别的任务。

BP网络一般结构由输入层、隐含层和输出层组成。学习过程中，输入信息首先从输入层经隐含层单元处理后传向输出层，每一层神经元的状态只影响下一层的神经元的状态。在输出层计算误差并转入反向传播，将误差信号沿原来的神经元连接通路返回并逐一修改各层神经元连接的权系数。通过反复迭代，直至信号误差达到允许范围，从而获得分类规则。各层神经元工作方法描述如下(秦其明和陆荣建，2000)：

设x_i为第i个输入节点的输入,那么隐含层第j个神经元的输出为y_j，则：

$$y_j = f\left(\sum_i W_{ij}x_i + \theta_j\right) \tag{2}$$

式中，W_{ij}为输入层第i个神经元和隐含层第j个神经元之间的权系数；θ_j为第j个隐含节点对应的阈值；本文传递函数采用Sigmoid函数,其形式为：

$$f(x) = 1\Big/\left(1+\exp\left(-\frac{x}{\theta_0}\right)\right) \tag{3}$$

式中，θ_0的作用是调节Sigmoid函数的形状。输出层第k个神经元的输出为O_k：

$$O_k = f\left(\sum_j V_{kj}y_i + \sigma_k\right) \tag{4}$$

式中，V_{kj}为隐含层第j个神经元和输出层第k神经元之间的权系数；σ_k为第k个输出节点对应的阈值。每次迭代后按误差下降梯度最大方向调整权重矩阵，学习速率由用户给定。在输出层计算输出和真值的误差，误差函数ε由式(5)给出：

$$\varepsilon = \frac{1}{2}\sum_{i=1}^{N}\sum_{k=1}^{p}(O_{ik} - T_{ik})^2 \tag{5}$$

式中，O_{ik}为实际输出；T_{ik}为希望输出；P为输出层神经单元个数；N为样本个数。

从LiDAR点云提取纹理特征进行分类的数据工作流程如图2所示：

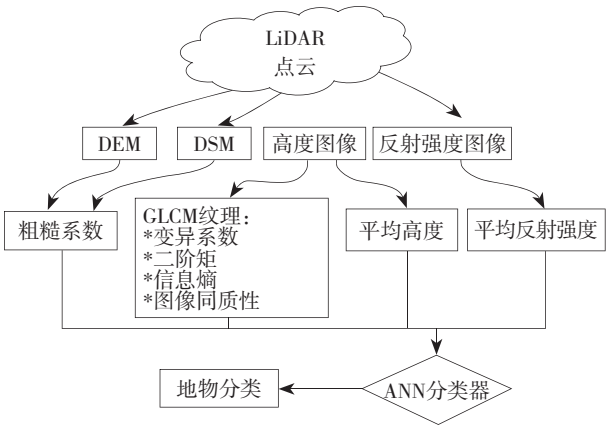

图2 工作流程

3 实 验

3.1 研究区域

选取珠江三角洲滨岸地带作为研究区域，实验区约2000 m × 1500 m的范围。区域为农业耕作区，地势平缓，平均地面起伏小于2° 。研究区域内有一个小规模的村落，人工建筑的平均高度小于10 m，与高大树木高度相仿且有相互遮叠。水体包括一条溪流与少量水塘；溪流有明显的沟槽特征。区域内裸地、草地与有作物的农田交错分布。

3.2 数据处理

LiDAR数据采集于2006-11-14，采集系统为Leica Airborne Laser Scanner 50，使用近红外波段激光发生器，数据采集于同一航线。数据为一次反射回波记录。采用UTM投影，航线上水平分辨率0.78 m，垂向分辨率0.15 m。区域内最大高差为13.16 m，其中高度低于6 m的点数占94%。激光反射强度以10个等级记录。首先利用TerraSolid软件包对点云进行分割，采用窗口最大斜率阈值法将点云分割为地面点和非地面点两个部分。初始分割窗口20 m × 20 m，迭代角阈值为小于2° 。随后分别利用地面点和全部点云按照0.8 m格网生成DEM表面和DSM表面。使用TerraScan软件，按照0.8 m的间隔分别用高程、反射强度值输出灰度图像，并拉伸到全灰度尺范围(图3)。

纹理采样窗口经过多次实验后采用7 × 7的检测窗口。窗口对应地面5.6 m × 5.6 m的范围，与研究区域内建筑、独立树木的覆盖物相仿或略小。实验结果也表明7 × 7卷积对所选的地面类型取得的效果最好。按照表1方法计算4个纹理特征，地面粗糙度由1式求得。4种GLML纹理和粗糙系数图像如图4所示：

(a) (b)

图3 从LiDAR点云导出的灰度图

(a)高度图像；(b)反射强度图像

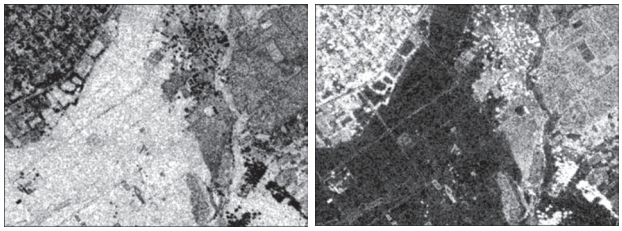

(a) (b)

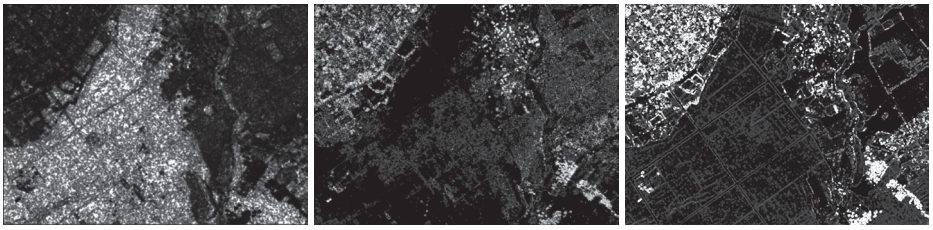

(c) (d) (e)

图4 4种地面纹理特征

(a)信息熵(*En*)；(b)同质性(*H*)；(c)二阶矩(*ASM*)；(d)变异系数(*V*)；(e)地面粗糙系数(C_p)

3.3 神经网络的训练和分类

建立3层BP-ANN ，计算程序由C#语言开发实现。将得到的4种GLCM高度纹理、平均强度、平均高度和地面粗糙系数共7个特征对应输入层7个神经元；隐层为4个神经元，该数目由经验确定；输出层5个神经元对应5种目标类型。训练样本按均衡样本采样，即要求各个类型所包含的样本数量大致相当。根据地面样本计算出的平均变换离散度为1.96，有较好的统计可分性。后向传播神经网络计算过程中采用Sigmoid激励函数，学习速率0.1。随后用训练集训练网络，完成训练后，将工作集输入网络进行分类。

4 结果与分析

4.1 实验结果

分类结果如图5(a)，误差混淆矩阵如表2。分类结果的总体精度为90.22%，工作误差最大的类型为建筑，但准确率也达到了79.6%；裸地和水体两类型取得了100%的工作精度，这种情况与水体的绝对高程低、裸地没有地面覆盖物具有较小的地面起伏有关。此外，还通过目视观察发现分类误差主要集中在建筑—林地的划分中，特别是在图5(a)的左上部。由于该位置的建筑物大多为小面积低矮的独立房屋，高度与林地相仿；对象边缘处计算得到纹理值也相近，BP-ANN分类时很容易相互混淆。沿着溪流沟谷分布的稀疏草地被识别为裸地；溪流上游流水覆盖的面积较小且成细条状分布，在纹理检测中无法填充满一个完整的纹理检测窗口，因而无法被使识别；其他连续水体均能够被有效的识别出来。

我们也用最大似然法(ML)对该区域进行了分类(图5(b))，并计算了ML分类器的误差混淆矩阵(表3)。可以看到两种分类方法都能够较好的识别地面覆盖类型。BP-ANN分类的总体精度比ML分类精度86.75%高出约3.5%，BP-ANN分类结果Kappa系数为0.877，

也比ML分类结果的Kappa系数0.832高。此外，ML分类得到的图斑要更为破碎，特别是建筑—林地、草地—裸地混杂小斑块较BP-ANN分类图更多，表明BP-ANN分类器有更好的多属性分析和类内综合能力。从表2、表3还可以看到，两个分类器误分样本的类型分布也有较大差异。由于建筑与林地有较多的相互叠掩且高度相仿，两个分类器在建筑类上都得到最小的分类精度，BP-ANN的精度为79.6%，而ML分类器的误差几乎全部集中在将建筑分为林地，该类别的判定精度仅为22.22%，判定几乎失效。BP-ANN分类器在林地、草地类型上都有误差，判定精度分别为72.3%和97.4%，略小于ML分类器。总体来说，BP-ANN的稳健性和容错性能均优于ML分类器。

表2 BP-ANN分类误差混淆矩阵

	建筑	水体	林地	草地	裸地
建筑	43	0	18	2	0
水体	0	46	0	0	0
林地	8	0	47	0	0
草地	3	0	0	76	0
裸地	0	0	0	0	74
合计	54	46	65	78	74

注：总体精度为 90.22%，Kappa为0.877

表3 ML分类误差混淆矩阵

	建筑	水体	林地	草地	裸地
建筑	12	0	0	0	0
水体	0	46	0	0	0
林地	35	0	65	0	0
草地	7	0	0	78	0
裸地	0	0	0	0	74
合计	54	46	65	78	74

注：总体精度为86.75%，Kappa为0.832

4.2 LiDAR与多光谱影像分类的一致性对比

LiDAR数据地面分类主要依赖地面对象的高度分异；对反射强度信号的辐射分辨率和波谱分辨率都较低，包括ALS50传感器在内的大多数LiDAR接收设备仅能划分出几十个辐射等级(本文的LiDAR数据只有10个辐射通量等级，难以用反射强度直接进行分类)。目前地面调查的主要手段还是常规多光谱数据，实际工作中LiDAR也常常会与多光谱数据相互补充或参照。因此我们也将该地区的多光谱影像进行了地物分类，并和LiDAR高度纹理分类结果进行了比较。

选用了该地区的ALOS影像。影像采集时间约晚于LiDAR数据2个月，由ALOS AVNIR2和PRISM传感器成像，分别为4波段多光谱影像和3通道全色影像，对地分辨率分别为10 m和3 m。对ALOS影像采用Brovey变换方法进行融合效果较好(柳文祎，2008)，融合后的图像按照0.8 m进行重采样。对ALOS影像用最大似然法进行分类。分类结果如图6。

从LiDAR分类结果中每个类型随机抽取100个像元，共500个像元，比对它们在ALOS影像和LiDAR高度图像中分类结果。对比的分类误差矩阵如表4，表中显示每个类型之间都有交叉，共有264个像元的两种分类属性一致，占总数的52.8%。除了建筑类外，其他类型LiDAR分类与光谱分类的一致性都在60%左右。目视比较图5(a)和图6，发现全图误差较大区域主要集中在左上角区域的建筑—植被分类中。实地调查表明，该区域大多数建筑单体面积较小且被林木部分遮盖，在光学影像的分辨率低于LiDAR高度图像的情况下，有较多的混合像元被识别为植被。

我们注意到，预先设定的地物类型与两种分类结果的一致性有很大的关系。例如，光谱分类很难将低矮灌丛、林地和茂密的草地分辨出来。如果把林地和草地两类型合并为植被类来考察，LiDAR和ALOS分类在植被这一类型上的一致性可达到76.5%。此外，在LiDAR图像中不能很好被识别的硬质路面或空地，却能在光谱分类中被识别出来。

LiDAR与光谱数据两种数据获取物理机制的差异、数据采集精度以及预设分类方案都会的影响最终分类结果的一致性。本文的实验是为了验证LiDAR分类的有效性，适合的分类方案和地面条件是两者可比的必要条件。在其他地面环境或分类条件下，LiDAR和光谱分类结果也可能完全不可比。因此，同时使用LiDAR和光谱数据进行分类的目的是为了更好理解地面特征和提高分类精度，而不能简单的要求获得较高的分类一致性。

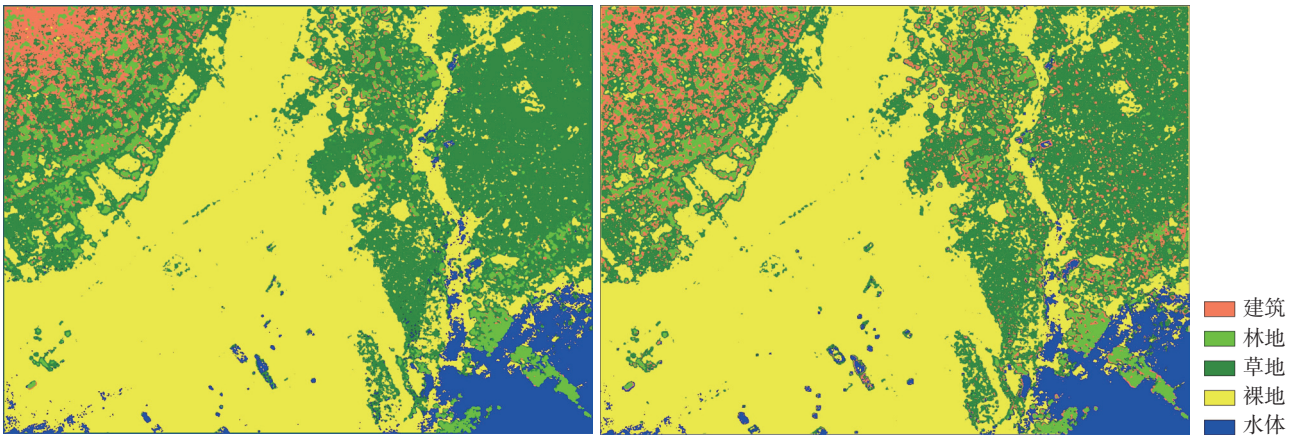

(a) (b)

图5 分类结果

(a) BP-ANN分类结果；(b)ML分类结果

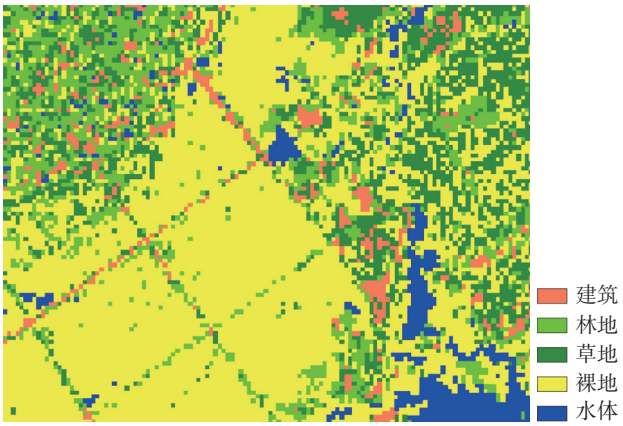

图6 ALOS影像分类

表4 ALOS影像和LiDAR高度图像分类一致性

		LiDAR分类						一致性
		建筑	林地	草地	裸地	水体	植被*	
光谱分类	建筑	23	4	11	18	4	15	0.23
	林地	40	67	17	11	5	153**	0.67
	草地	24	15	54	6	9		0.54
	裸地	8	11	16	61	23	27	0.61
	水体	5	3	2	4	59	5	0.59

*由草地、林地两类型样本合并为植被类

**植被类型的抽样像元总数为200，一致性为0.765

5 结 论

(1)LiDAR点云数据提供了地面高程、高差以及地面反射强度的信息。本文将离散点云转换为高度灰度图像和强度灰度图像后，利用图像分割技术，从高度纹理特征中提取分类规则。高度纹理分类所利用的主要信息源与点云斜率阈值分割是一致的，都要利用激光足点间高程变化的信息；但高度纹理具有更强的容错性和模糊特征，更适用于复杂地表对象的识别。研究中提出结合地面粗糙系数和反射强度信息对地物进行分类。实验表明：在不使用其他数据源的情况下，整合了反射强度、地面高度和地面粗糙度信息的LiDAR灰度图像，也能够对地面覆盖物进行有效的识别和划分。

(2)利用LiDAR高度纹理进行地物识别比直接利用离散点云提取高程变异信息更加有效；而且高程纹理所反映的地面对象特征也比离散点云的高度分布特征更为深刻和易于理解。利用ANNs从高维特征空间中寻找分类规则是一种有效的LiDAR数据分割方法，分类精度高于最大似然法。在LiDAR地面覆盖物分类的工作中，智能计算方法更能够适应高度纹理的特征识别任务，并获得较高的分类精度。

(3)在高度纹理分类与光谱分类结果的比对中，类间一致性分布在23%—67%之间，总体一致性为52.8%，LiDAR分类与光谱分类结果不能直接用以相互参照。但合并林地和草地两类型为植被后，LiDAR高度纹理和光学影像取得了76.5%的一致性(表4)。考虑实验中使用数据分辨率不一致而导致的误差，在该类型上取得的实际一致性可能会更高。因此，在地面类型预设和分类机理同时满足被光谱和LiDAR识别条件的情况下，这两种分类结果可比。

(4)由于LiDAR数据源的信息主要集中在地面对

象的高度分异，预先设定的地物类型在高度特征上必须是可分的。此外，依赖纹理特征的分类也隐含了地物必要的先验知识。本文的实验区域面积较小，地面结构也相对简单，因此依靠经验设定地物类型就能取得较好的效果。但在复杂环境或用户对地面高度变化的经验不足的情况下，依赖人工经验可能会引起较大的误差。引入其他智能分类方法并发展基于对象的LiDAR高度纹理识别技术有克服上述问题的潜力，这也是下一步研究的方向。

志　谢　黎夏教授组织的“985工程−GIS与遥感的地学应用项目实验平台”为研究工作提供了良好的研究环境，并给出大量有益的指导意见；吴秋生硕士、艾彬博士、何晋强博士在文档资料收集和实验中提供了大量帮助。

REFERENCES

Axelsson P. 1999. Processing of laser scanner data-algorithms and applications. *ISPRS Journal of Photogrammetry and Remote Sensing*, **54**: 138–147

Dimitrios C and Keith A. 2007. A texture-based technique for DEM generation from LIDAR data. Proceedings of SPIE, 6550, 65500O. DOI:10.1117/12.719935

Filin S. 2002. Surface clustering from airborne laser scanning data. *International Archives of the Photogrammetry, Remote Sensing and Spatial Information Sciences*, **34** (Pt. 3A): 119–124

Franklin S E, Maudie A J and Lavigne M B. 2001. Using spatial co-occurrence texture to increase forest structure and species composition classification accuracy. *Photogrammetric Engineering & Remote Sensing*, **67**(7): 849–855

Haralick R M.1986. Statistical Image Texture Analysis. Handbook of Pattern Recognition and Image Processing. New York: Academic Press

Jungho I, John R and Michael E. 2008. Object-based land cover classification using high-posting-density LiDAR data. *GIScience & Remote Sensing*, **45**(2): 209–228

Kraus K and Pfeifer N. 1998, Extraction of buildings and trees in urban environments. *ISPRS Journal of Photogrammetry and Remote Sensing*, **53**: 193–203

Liu W Y, He G J, Zhang Z M and Liu H C. 2008. Comparison of fusion algorithms for ALOS panchromatic and multispectral images. *Science Technology and Engineering*, **8**(11): 2864–2869

Liu X P, Li X, Liu L and He J Q. 2008. An innovative method to classify remote-sensing images using ant colony optimization. *IEEE Transactions On Geoscience and Remote Sensing*, **46**(22): 4198–4208

Maas H G. 1999. The potential of height texture measures for the segmentation of airborne lasers canner data. Fourth International Airborne Remote Sensing Conference and Exhibition. Ottawa: 21st Canadian Symposium on Remote Sensing: 154–161

Minh Q, Nguyen P, Atkinson M and Hugh G L. 2005. Superresolution mapping using a hopfield neural network with LIDAR data. *IEEE Geoscience and Remote Sensing Letters*, **2**(3): 366–370

Poonam S and Tiwari H P. 2008. Use of laser range and height texture cues for building identification. *Journal of the Indian Society of Remote Sensing*, **36**: 227–234

Qin Q M and Lu R J. 2008. Satellite image classification based on fractal dimension and neural network. *Acta Scientiarum Naturalium Universitatis Pekinensi*, **36**(6): 858–864

Raber G, Jensen J R, Hodgson M E, Tullis J A, Davis B A and Berglund J. 2007. Impact of LiDAR nominal posting density on DEM accuracy and flood zone delineation. *Photogrammetric Engineering & Remote Sensing*, **73**(7): 793–804

附中文参考文献

柳文祎，何国金，张兆明，刘慧婵．2008．ALOS全色波段与多光谱影像融合方法的比较研究．科学技术与工程，8(11): 2864–2869

秦其明，陆荣建．2000．分形与神经网络方法在卫星数字图像分类中的应用．北京大学学报(自然科学版)，**36**(6): 858–864